Superconductor Science and Technology

A 1.2-T canted cosΘ dipole magnet using high-temperature superconducting CORC® wires

To cite this article before publication: Xiaorong Wang *et al* 2019 *Supercond. Sci. Technol.* in press https://doi.org/10.1088/1361-6668/ab0eba

A 1.2-T canted $\cos\theta$ dipole magnet using high-temperature superconducting CORC® wires

Xiaorong Wang[1], Daniel R. Dietderich[1], Joseph DiMarco[2], William B. Ghiorso[1], Stephen A. Gourlay[1], Hugh C. Higley[1], Andy Lin[1], Soren O. Prestemon[1], Danko van der Laan[3,4], Jeremy D. Weiss[3,4]

[1] Lawrence Berkeley National Laboratory, Berkeley, CA 94720, USA
[2] Fermi National Accelerator Laboratory, Batavia, IL 80510, USA
[3] Advanced Conductor Technologies, Boulder, CO 80301, USA
[4] University of Colorado, Boulder, CO 80301, USA

E-mail: xrwang@lbl.gov

Abstract. $REBa_2Cu_3O_x$ (REBCO, RE = rare earth elements) coated conductors can carry high current in high background fields, in principle enabling dipole magnetic fields beyond 20 T. Although model accelerator magnets wound with single REBCO tapes have been successfully demonstrated, magnet technology based on high-current REBCO cables for high-field accelerator magnet applications has yet to be established. We developed a two-layer canted $\cos\theta$ dipole magnet with an aperture of 70 mm using 30 m long commercial Conductor on Round Core (CORC®) wires. The 3.1 mm diameter CORC® wire contained 16 commercial REBCO tapes with a 30-μm thick substrate. The magnet was tested at 77 and 4.2 K. It generated a peak dipole field of 1.2 T with 4.8 kA at 4.2 K with neither thermal runaway nor training. Reasonable geometric field quality and strong magnetization-current effects with multipole decay were observed. Our work demonstrated a feasible high-temperature superconducting magnet technology as a first step toward a new accelerator magnet paradigm that will enable high-field inserts for next-generation circular colliders and stand-alone magnets that can operate over a wide temperature range for a broad range of applications.

1. Introduction

To reach a dipole field of 20 T and beyond, high-temperature superconducting (HTS) materials such as $Bi_2Sr_2CaCu_2O_{8+x}$ (Bi-2212) and $REBa_2Cu_3O_x$ (REBCO, RE = rare earth elements) are required because of their superior current-carrying capability in a background field of 45 T or higher [1, 2]. Recent progress in Bi-2212 magnets can be found in [3, 4]. Here we focus on REBCO coated conductors with several unique features that can have significant impact on future accelerator magnet technology and its applications.

REBCO coated conductor, on a short-sample scale, has demonstrated over 5 kA mm^{-2} engineering current density (J_e, transport current per unit conductor cross

sectional area), the highest among all technical superconductors at 4.2 K, 14 T [5]. A series of record magnetic fields has been demonstrated in REBCO solenoid magnets [6–9]. Like NbTi, REBCO conductors do not require heat treatment, significantly simplifying the magnet fabrication. The material's unique capability of carrying high current over a wide temperature range with high thermal stability can enable magnet applications with versatile cooling methods beyond liquid helium.

High-field accelerator magnets require high-current cables, e.g., 10 – 20 kA at nominal operating temperature and fields [10]. Such operating currents require REBCO tapes to be bundled into cables, such as Roebel [11], twisted stacked tape [12] and Conductor on Round Core (CORC®) cables [13]. The compact cable configurations typically lead to a J_e of at least 300 A mm^{-2} at operating conditions.

Although several model accelerator magnets wound from single REBCO tapes have been demonstrated [14–18], there are only a few reports on the development of magnet technology using high-current REBCO cables. The European EuCARD2 program, a large collaborative effort led by CERN, is focusing on REBCO Roebel cables for accelerator magnets [19, 20]. In the program, a 3.1 T dipole field was demonstrated in a 40 mm aperture at 5.7 K based on the Aligned Block design [21, 22]. A 4.52 T dipole field was demonstrated with racetrack coils wound with a double-layer REBCO tape at 4.2 K [23], although the magnet does not have a clear aperture.

CORC® cables are fully isotropic with respect to mechanical bending and in-field performance. They can also be produced at long lengths without the need to precisely pattern REBCO coated conductors as required for Roebel cables. In addition, CORC® cables and wires‡ are resilient to mechanical transverse compressive [24] and axial tensile stresses [25] such that it may not be necessary to impregnate the interior of the cable to provide the crucial mechanical support [26]. One advantage of Roebel cables is the higher in-field J_e with a small bending radius of several mm along the broad surface of the cable, although CORC® wires are quickly catching up [27]. The potential of round REBCO wires was also demonstrated by a 1.6 mm diameter REBCO wire with a J_e of 454 A mm^{-2} at 15 T, 4.2 K and a bending radius of 15 mm [28].

To demonstrate and exploit the potential of REBCO conductors for future high-energy physics accelerator applications, the U.S. Magnet Development Program [29], funded by the U.S. Department of Energy's Office of High Energy Physics, together with its industry partner Advanced Conductor Technologies LLC (ACT), is developing accelerator magnet technology for REBCO conductors based on CORC® wires to demonstrate a 5 T dipole field at 4.2 K, followed by testing the magnet in an external dipole field.

Following the first demonstration of a 3-turn canted $\cos\theta$ (CCT) design using CORC® cables [30, 31], we reported a similar concept using CORC® wires [32]. Although several 3-turn CCT magnets were successfully developed to prove the principle,

‡ Here we use the word "wires" to describe multi-tape cables of small diameter.

they used only short CORC® wires of less than 3 m in length and several questions that are critical for accelerator magnet applications remain open. In particular,

- Can we make magnets with long CORC® wires that can be scalable to larger accelerator magnets operating at a total field of 20 T?
- Is the magnet performance as expected and how can CORC® wires be further optimized to improve the winding efficiency of the CCT magnet?
- What is the field quality of CORC® CCT magnets?
- What are the open issues to be addressed?

As a first step to address these questions, we developed and tested a dipole magnet, C1, using low-J_e CORC® wires with a target dipole field of 1 T. It has two layers with 40 turns and used 30 m long CORC® wires. Here we report the detailed magnet design, fabrication, test results and recommendations on conductor and magnet improvement that should be taken into account during further development of CORC® CCT accelerator magnets. The successful demonstration of the C1 magnet clearly indicated that the CCT concept with round CORC® wires is feasible for HTS accelerator magnets. It is a first step toward practical and reliable HTS magnets as a new paradigm for superconducting accelerator magnet technology that will enable next-generation circular colliders at the energy frontier and stand-alone magnets for applications such as injection chain [33], high radiation environment [34] and ion beam therapy [17, 35].

2. Magnet design and fabrication

2.1. CORC® wire

ACT manufactured the CORC® wires using commercial REBCO tapes with 30 μm thick substrate manufactured by SuperPower Incorporated [13]. The wires contained 16 tapes of 2 mm width and had an outer diameter of 3.16 mm. Two pieces of 25 m long CORC® wire were manufactured. Table 1 outlines the main parameters of the CORC® wire used for the C1 magnet.

2.2. Magnet design

Magnet C1 follows the CCT concept that was first introduced in 1970 [36] and further developed by various groups [37–41]. The design has two main advantages: first, the conductors are embedded in the magnet mandrel to intercept the Lorentz forces on each cable and prevent the accumulation of forces on the conductors that can impart high stress and limit the conductor performance. Second, the current density follows a natural $\cos\theta$ distribution and thus the design promises excellent geometric field quality. The CCT design is also being pursued for Bi-2212 HTS dipole insert magnets [42, 43], high-field Nb_3Sn accelerator magnets [44, 45], a gantry magnet for proton therapy [46], and NbTi corrector magnets for the High-Luminosity LHC [47].

Table 1. Main parameters for the C1 CORC® wires.

	Unit	Value
Tape vendor	-	SuperPower Inc.
Tape width	mm	2
Substrate thickness	μm	30
Cu plating thickness	μm	5
Layers	-	8
Tapes per layer	-	2
Average tape I_c, 77 K, self-field	A	70
Piece length	m	25
Insulated wire diameter	mm	3.16
Polyester insulation thickness	μm	30
Diameter of Cu core	mm	2.34
Cu to non-Cu ratio	-	1.63
Termination length	mm	170
Termination diameter	mm	6.35

The C1 magnet has two layers with a clear aperture of 70 mm to allow for an anticryostat for field quality measurements (figure 1). The assembly of both layers adds their dipole fields and cancels the solenoid fields in the aperture. It follows the same design as C0a, a 3-turn magnet [32], but with 40 turns per layer. The conductor tilt angle was determined by the minimum allowed bending radius of the CORC® wires used for C1. Table 2 outlines the main design parameters for C1.

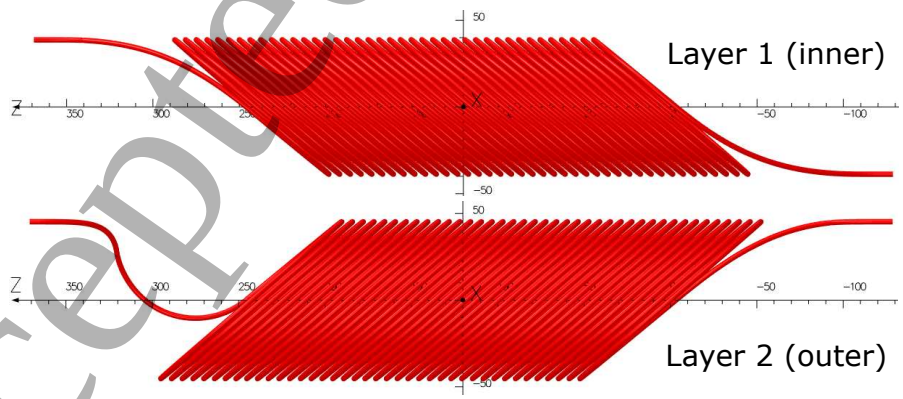

Figure 1. Side views of two coils for the C1 magnet. Lead end is located at the negative z axis. The dimensions are in mm.

The mandrels for both layers were 3D printed using non-magnetic material called Acura® Bluestone®. The radial clearance between two layers was 1 mm for convenient assembly of the two layers and to accommodate the tolerance of printed parts.

Table 2. Main design parameters for the C1 magnet.

Design parameters	Unit	Value
Clear aperture	mm	70
Magnet outer diameter	mm	94
Turns per layer	-	40
Layers	-	2
Radial clearance between layers	mm	1.0
Groove diameter	mm	3.5
Rib thickness	mm	0.5
Spar thickness	mm	2.0
Conductor tilt angle	degree	40
Minimum bending radius of the conductor center line	mm	25
Wire pitch length over one turn	mm	6.22
Mandrel length	mm	500
Mandrel material	-	Accura® Bluestone®
Wire length for Layer 1	m	14.0
Wire length for Layer 2	m	15.8
Short-sample prediction (SSP) at 4.2 K, self-field	kA	4.624
Aperture/conductor field at the SSP	T	1.17/1.39
Inductance	mH m^{-1}	0.53
Stored energy at the SSP	kJ m^{-1}	5.67

2.3. Coil winding and termination installation

An important design feature for the C1 magnet was the tilted groove that allowed the continuous winding of the CCT coils with minimum handling of CORC® wires. Earlier 3-turn magnets showed that the tilted groove design could facilitate manual coil winding [32]. To demonstrate a technique of winding long conductors that will be required for larger coils, a prototype winding table that complemented the tilted grooves on the mandrel was developed by H. Higley at LBNL. It features a rotating wheel where a back-tensioned wire spool is mounted. By tilting the mandrel, the grooves become planar for the wire to enter from the same plane. Figure 2 shows the winding of a 40-turn prototype coil with the table. The mandrel height was adjusted during winding to maximize the groove clearance for the incoming wire.

The CORC® wires were terminated with a 170 mm long oxygen-free high-conductivity Cu tube at each end. One termination was installed before coil winding, while the second one was installed after the coil was wound and the CORC® wire was cut to length. Inside the CORC® termination, every layer of REBCO tapes was exposed to direct contact with the Cu tube for better current transfer. The tube was then heated to 195°C for a duration of 5 minutes to fill with molten Indium solder. The Indium solder helped to reduce the contact resistance between REBCO tapes and Cu tube and

Figure 2. (Multimedia) Using a winding table, Hugh Higley (left) and Andy Lin (right) tested winding a prototype of the 40-turn C1 inner layer.

the overall termination resistance [27, 48].

The coil winding procedure included first positioning and strain-relieving the lead end conductor into the groove between the mandrel edge and the first turn (figure 1). The winding then started from one end toward the other end of the mandrel. The return end conductor was again manually positioned into the groove. We successfully wound both layers of C1 using the winding table with total CORC® wire length of 30 m. Figure 3 shows the completed coils before assembly. A minimal tension of 10 N was applied on conductors during winding.

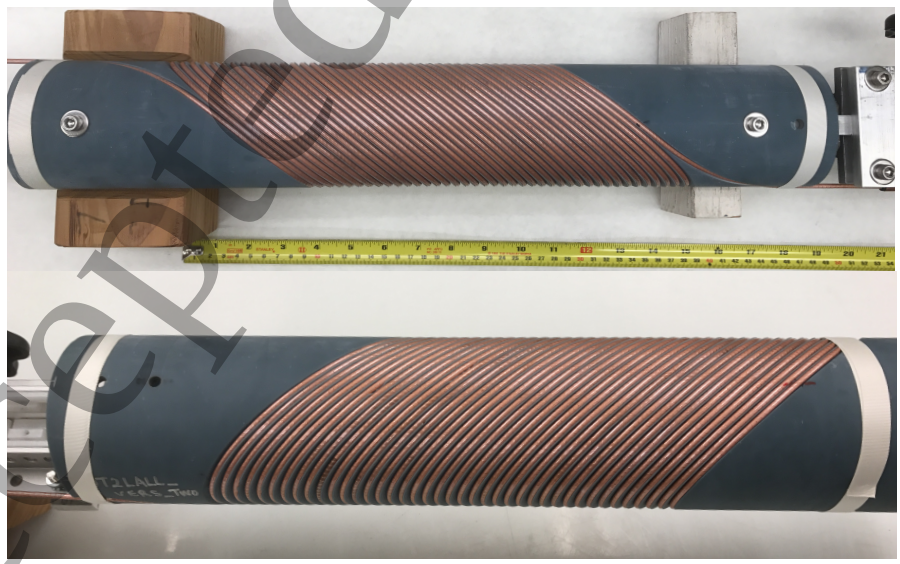

Figure 3. Layer 1 (top) and 2 (bottom) of C1 after winding. Cu instrumentation wire was wound next to the conductor in the groove.

Instrumentation wires were co-wound next to the conductor into the groove to reduce the inductive voltage during the measurements. Finally, 3M® adhesive electric

tape was wrapped around the coil to constrain the conductors and instrumentation wires. The coils were not impregnated.

2.4. Magnet assembly and joint fabrication

Both magnet layers were assembled and locked in both azimuthal and longitudinal directions with non-magnetic stainless steel metal pins through the alignment holes at the mandrel ends. The assembled magnet was then anchored to a G10 board with non-magnetic clamps. Shims were used to fit in the 1 mm radial clearance to help center the inner layer with respect to the outer layer. Figure 4 shows a 1:1 mockup assembly of C1 and the electrical joints at both magnet ends.

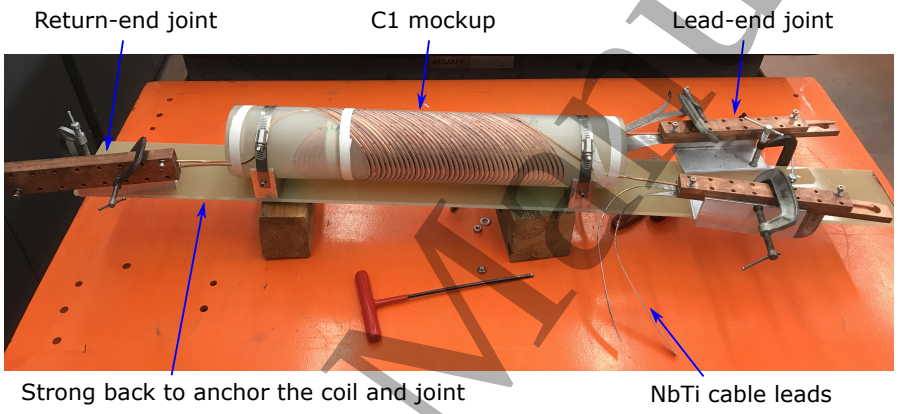

Figure 4. A 1:1 mockup model for C1. The model was used to develop and verify the assembly concept and to determine and confirm the required conductor length as provided by the CAD model. The winding of Layer 1 (inner layer) can be seen through the mandrel of Layer 2.

The magnet had three electrical joints: two at the lead end and one at the return end (figure 4). For each joint, the Cu termination for the CORC® wire was sandwiched between a pair of Cu blocks with Indium foil. At the return end, the lead conductors from both layers were connected in a "praying-hand" joint. The lead conductors and joints were slightly bent away from the magnet to allow an anti-cryostat to be inserted for field quality measurements.

The lead-end joints had NbTi cables soldered on one side of the Cu block (figure 4). The NbTi cables and additional Cu braids connected the lead-end joint to the vapor-cooled leads from the cryostat header.

3. Experimental details

3.1. Test setup

The voltage across each layer was used to measure the onset of the transition from the superconducting to normal state and to detect potential magnet quenches. Three voltage taps (VT) were installed inside or close to the Cu terminations (figure 5). VT0/5

were soldered to the Cu core outside the termination, VT1/4 were located in the center of the Cu termination and VT2/3 were located close to the edge of the Cu termination. Three voltage signals were measured for each layer: V_0 between VT 0 and 5, V_1 between VT 1 and 4, and V_2 between VT 2 and 3. The return-end joint voltage was monitored between the VT3 taps from both layers.

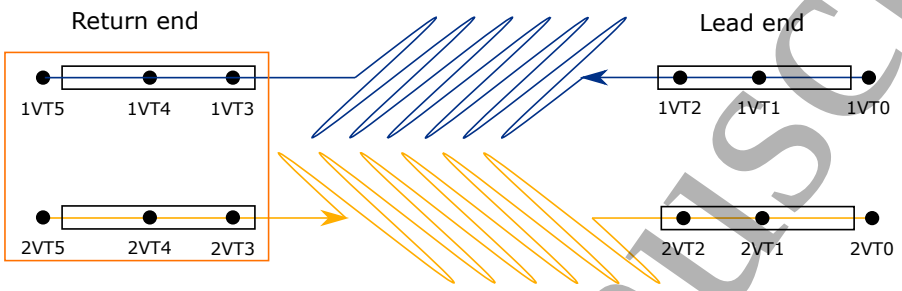

Figure 5. The voltage taps installed on each layer of C1. Black boxes are terminations. Current flows from Layer 1 to Layer 2 as indicated by the arrows. A praying-hand joint (orange box) connected both layers at the return end.

Two sets of instruments were used to measure the layer voltages. One was Keithley 2182A nanovoltmeters at a measurement frequency of 1 Hz. The amplified analog layer voltage signals, available from the nanovoltmeters, were used to trigger the quench detection system. The second was a National Instruments SCXI data acquisition system at a sampling rate of 1 kHz. Voltages across the NbTi cable, entire magnet, and vapor-cooled leads were measured with a Keithley 2001 digital multimeter.

The magnet was positioned vertically in a cryostat for both 77 and 4.2 K tests. The lead-end joints pointed upward toward the cryostat header. The liquid cryogen level was continuously monitored to ensure that the top of the lead-end joints submerged in cryogen during the tests. Two calibrated Cernox® temperature sensors monitored the temperature close to the magnet. One sensor was located close to the lead-end joints and the other one was located at the bottom of the cryostat.

An anticryostat was inserted into the magnet aperture to measure the field quality of C1. A printed-circuit-board rotating coil, developed at Fermi National Accelerator Laboratory [49], was used to measure the field quality. The measurement circuit in the probe is 100 mm long. The field harmonics were normalized to the dipole field and reported at the probe radius of 21.55 mm (reference radius, R_{ref}) in unit (1 unit = 10^{-4} dipole field).

3.2. Measurement protocol

To ensure that no significant degradation in the coil performance occurred after winding, we measured the voltage across each individual layer as a function of transport current at 77 K.

After assembly, the C1 magnet was tested at 77 and 4.2 K for both transport performance and field quality. All measurements were performed at self-field. The

transport performance of the magnet was first determined by measuring the voltage across each layer as a function of current.

Once the transport performance was determined, we performed the following field quality measurements: 1) scanning along the magnet bore to determine the multipole profile, and 2) measuring at the magnetic center during current ramping. The layer voltages and other signals were continuously monitored during the field quality measurements, while the cryogen level was maintained.

C1 went through four thermal cycles between room temperature and 77 or 4.2 K. The tests and their sequence are shown in figure 6.

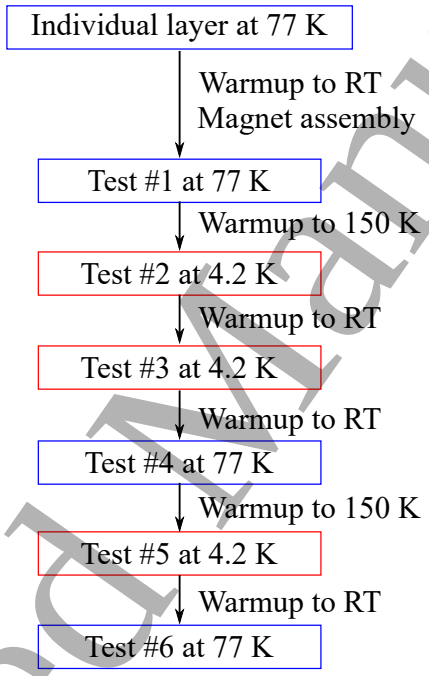

Figure 6. Test sequence of C1. RT means room temperature.

The cooldown rate was below 50 Kh^{-1} from room temperature to 77 K. A similar cooldown rate was used when the magnet was precooled with liquid nitrogen to around 150 K for the 4.2 K test. Afterwards, the rate was increased to 100 to 150 Kh^{-1} when cooling down to 4.2 K with liquid helium.

4. Test results

4.1. Transport performance at 77 K

The voltage-current $[V(I)]$ transition was first compared for each layer before and after they were assembled into the two-layer magnet (figure 7). The voltage V_2 for both layers was used because they were least affected by the current transfer from the Cu termination to superconducting tapes.

The transport performance of each layer decreased after the layers were assembled due to the increased magnetic field on each layer (57% increase on Layer 1 and 43%

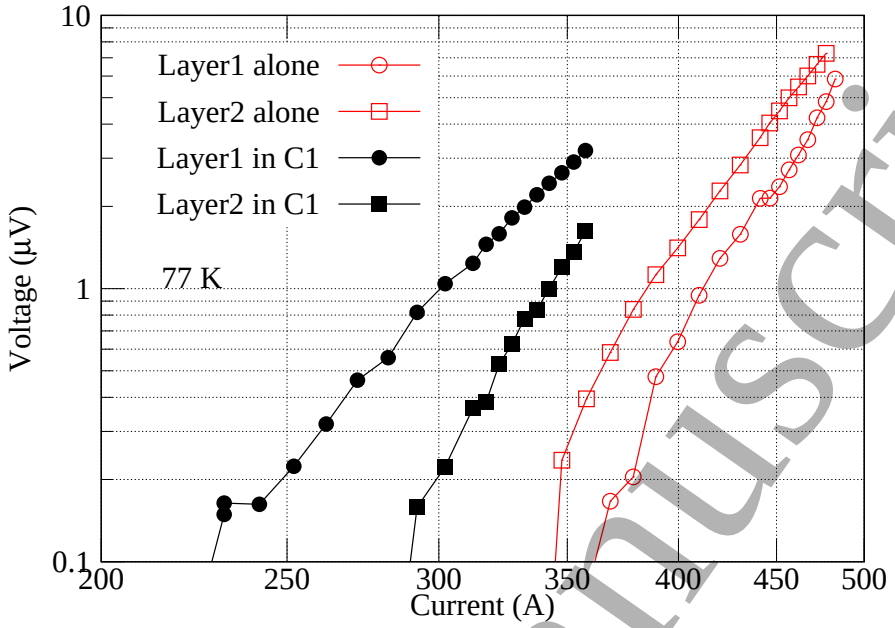

Figure 7. Layer voltage before and after the assembly of C1 at 77 K in self-field.

increase on Layer 2). To quantify this change, we report in table 3 the critical current of each layer as determined at a voltage criterion of 1 μV by fitting the $V(I)$ data with a power-law relation

$$V = V_c \left(\frac{I}{I_c}\right)^n, \tag{1}$$

where V_c is the voltage criterion and I_c the critical current at the voltage criterion. The fit range was up to 3 μV for Layer 1 and 2 μV for Layer 2. The voltage criterion would underestimate I_c compared to the electric-field criterion of 1 μV cm^{-1} which, typically used for HTS conductors, would correspond to a voltage of about 1.5 mV due to the 15 m length of the CORC® wire in both layers. The much lower criterion was used to prevent any chance of burnout due to localized dissipation [32].

Table 3. I_c and n value of Layers 1 and 2 defined at 1 μV voltage criterion before and after assembly into C1. 77 K, self-field.

	Layer 1		Layer 2	
	I_c (A)	n	I_c (A)	n
Before assembly	405	9.3	387	10.3
After assembly	293	6.1	340	10.8
Change	−27%	−36%	−12%	5%

4.2. Transport performance at 4.2 K

The layer voltage during the current ramps at a rate of 23 A s^{-1} at 4.2 K is shown in figure 8. Starting from 4.542 kA, the current was held for 10 s every 50 A up to 4.845 kA, the highest current tested during the 4.2 K test, and then ramped continuously down to 0 A at the same rate. A voltage of about 12 μV was measured over Layer 1 and about 17 μV over Layer 2 at the highest current, including an inductive component of around 5 μV during current ramping.

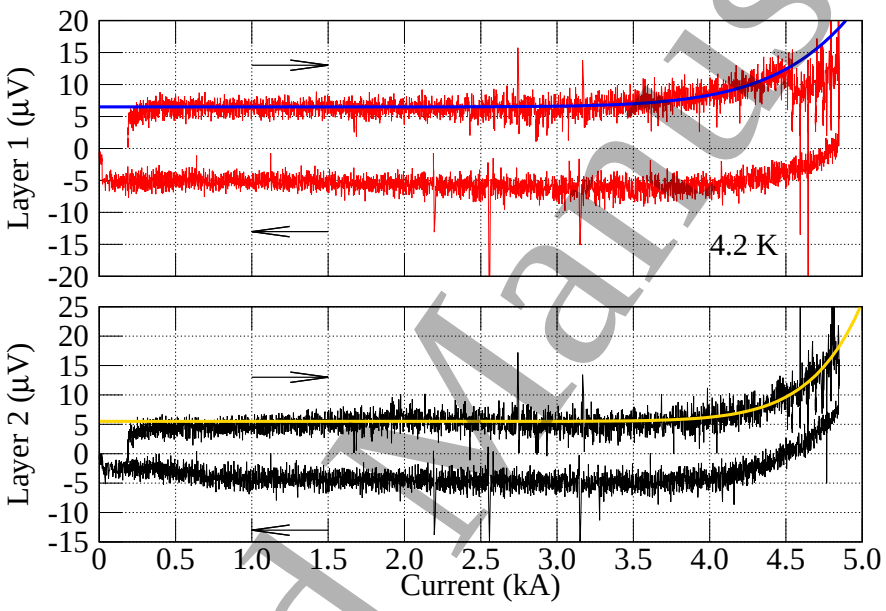

Figure 8. The layer voltage as a function of current during the ramp at 4.2 K. The arrows denote the direction of current ramp. The blue and gold smooth lines are the power-law fit for the $V(I)$ data during the up-ramp.

Equation (1) was used to fit the voltage measured over both layers during the up-ramp. Using a voltage criterion of 1 μV, Layer 1 started transitioning at 3.761 kA (81% of the short-sample prediction, see below) and Layer 2 at 4.094 kA. The n value was 9.9 for Layer 1 and 15.0 for Layer 2. Other 4.2 K tests showed a similar $V(I)$ profile.

The load lines that represent the magnetic fields on the conductor and within the aperture as a function of current are shown in figure 9. It also shows the expected wire performance, which is the critical current as a function of magnetic field of the wire estimated from the critical current of single tapes measured with a criterion of 1 μV cm^{-1} without self-field correction [32]. The conductor load line gives a short-sample prediction (SSP) of 4.624 kA. The magnet was able to carry a peak current of 4.845 kA without thermal runaway. The corresponding J_e in the wire was 618 A mm^{-2} at a minimum bending radius of 25 mm, 1.45 T and 4.2 K. The maximum dipole field in the aperture is 1.2 T at the peak current (figure 9). No training was observed between the tests.

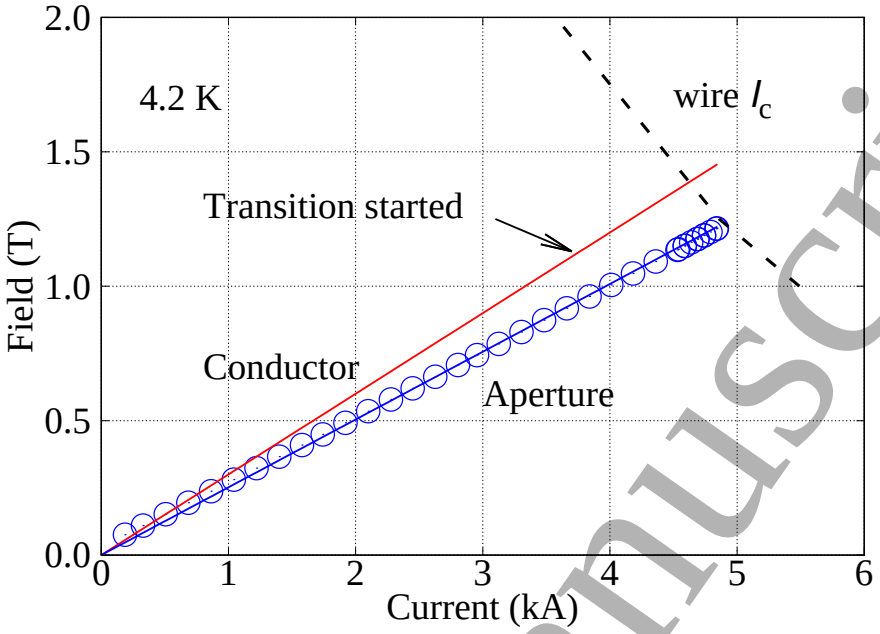

Figure 9. The load line for the field on the conductor (red line) and in the magnet aperture (blue line) for C1. The predicted short-sample current was 4.624 kA, the interception of the conductor load line and the expected wire $I_c(B)$ performance (black dashed line). Layer 1 voltage started rising at 3.761 kA. The peak transport current was 4.845 kA with a dipole field of 1.2 T in the aperture. The measured dipole field (blue circles) agreed with the calculation.

The layer voltage with a stair-step current profile between 4.542 and 4.845 kA is shown in figure 10. At each current step, the resistive layer voltages were stable or decaying following the initial reduction in the inductive voltage. The maximum resistive power generated was about 60 mW in Layer 2 and 40 mW in Layer 1.

We also held the current at 4 kA (510 A mm^{-2}) for 30 minutes when taking magnetic measurements. The layer voltage remained constant over the entire current plateau without thermal runaway. A total heat of 45 J was generated during the current plateau.

4.3. Joint performance

Figure 11 shows the voltage across the return-end joint measured across taps 1VT3 and 2VT3 (figure 5) as a function of current. The joint voltage showed a deviation from linear $V(I)$ behavior at around 100 A at 77 K and 2.5 kA at 4.2 K. The joint resistance was 333 nΩ at 77 K and 53 nΩ at 4.2 K based on the linear portion of the $V(I)$ data.

Figure 12 shows the voltage signals based on VT1 and VT2 taps (figure 5) for both layers with the linear resistive component removed. The voltage started rising at about 2 kA in the return-end termination of Layer 2, compared to 3.1 kA in the return-end termination of Layer 1. Figure 12 also shows that the superconducting to normal transition observed at the return-end joint was contributed by the transition in the first half of each termination (between voltage taps VT3 and VT4, figure 5), in particular

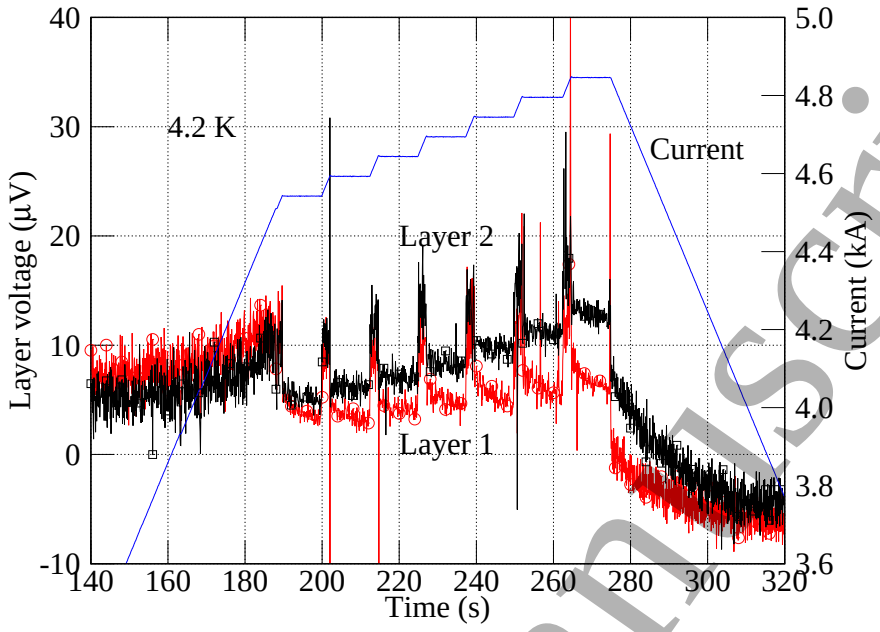

Figure 10. Layer voltage and magnet current as a function of time with the stepped current. Red line and open circles denote the voltage across Layer 1. Black line and open squares denote the voltage across Layer 2.

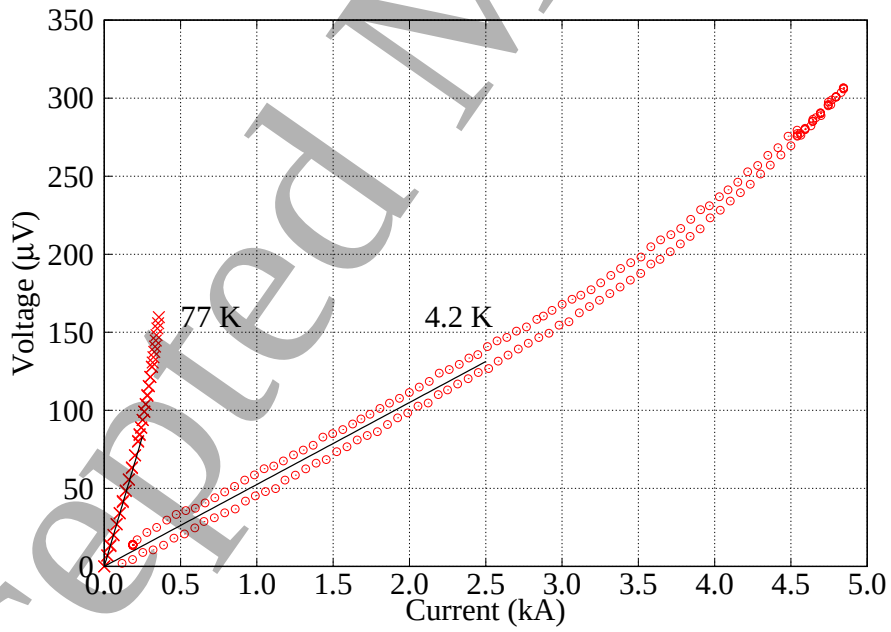

Figure 11. Voltage across the return-end joint as a function of current at 77 and 4.2 K. The slope of the solid line gives the resistance of the return-end joint.

between the voltage taps 2VT4 and 2VT3 in the return-end termination of Layer 2.

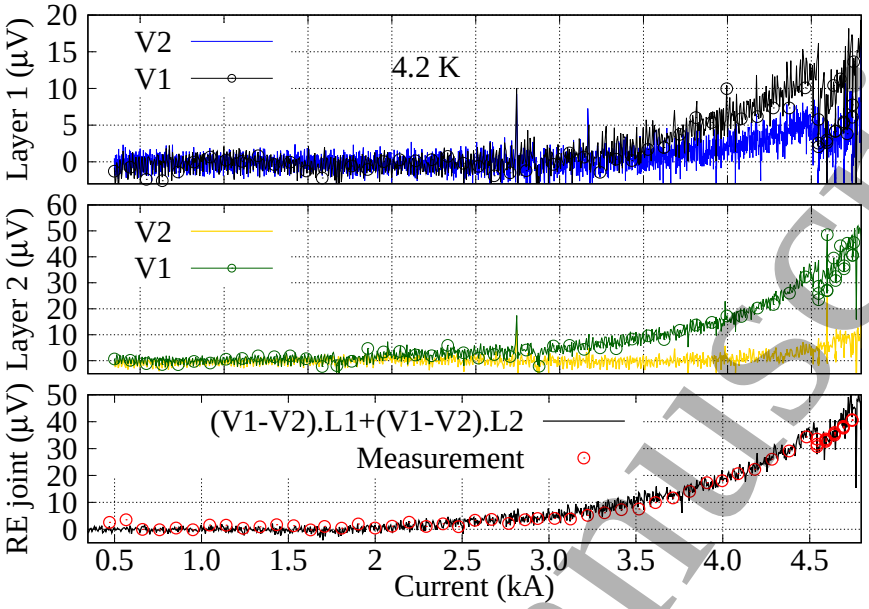

Figure 12. The voltage across each layer and the return-end joint as a function of current at 4.2 K. The linear resistive component was removed. The voltage inside the terminations from both layers added to the measured superconducting to normal transition in the return-end joint.

4.4. Transport performance after thermal cycles

In figure 13, we compare the layer voltage during the current ramp between all three 77 K tests performed with the same current ramping profile (see figure 6 for the test sequence). To quantify the change of current-carrying capability, we used a voltage criterion of 1 μV after removing the resistive voltage component below 200 A. A reduction in I_c by 2% in Layer 1 and 3% in Layer 2 was observed (table 4). The change in n value was negligible. Interestingly, the slope of the resistive foot below 200 A reduced from 5.9 nΩ during the first 77 K test to 1.7 nΩ during the second and third 77 K tests (figure 13 and table 4).

Table 4. Comparison of the I_c, n value and resistive slope (R) based on the V_2 voltage between three 77 K tests.

	Layer 1			Layer 2		
Test	I_c (A)	n (-)	R (nΩ)	I_c (A)	n (-)	R (nΩ)
1	293	6.1	5.9	340	10.6	−0.2
2	289	6.7	1.7	329	11.6	0.7
3	287	6.4	1.7	330	10.6	−0.4

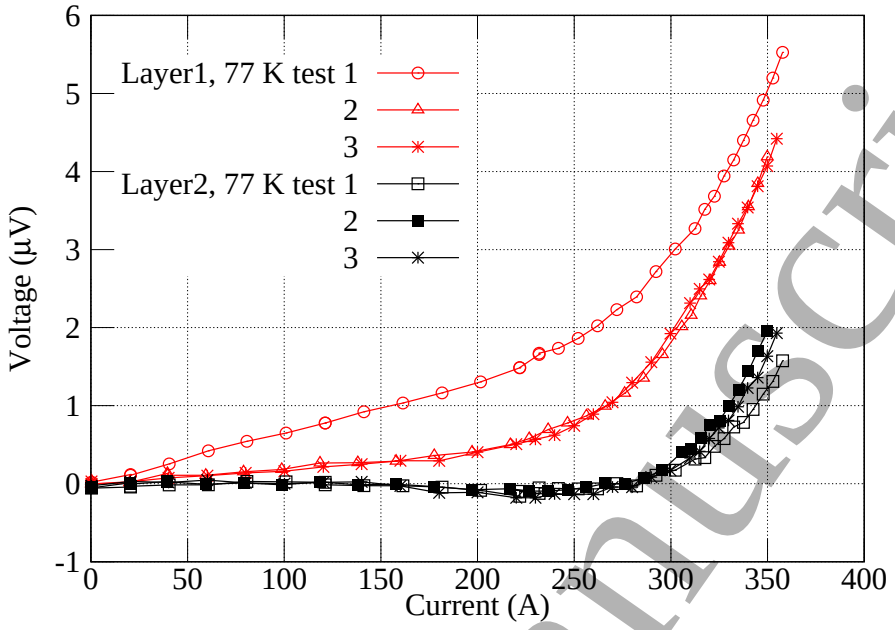

Figure 13. Comparison of the layer voltage V_2 as a function of current between three 77 K tests.

4.5. Field quality

Although the magnet was not impregnated and the conductors were allowed to move, magnet C1 provided a first opportunity to probe the field quality of CCT accelerator magnets made of CORC® wires.

Figure 14 shows the dipole transfer function (TF) and sextupoles along the magnet length at 0.1 kA at 77 K and 1 kA at 4.2 K with negligible Lorentz forces on conductors in both cases.

Both the dipole transfer function and sextupoles agreed reasonably well with the calculation based on the as-designed conductor positioning. For instance, within ± 20 mm of the magnetic center with relatively low impact from the coil ends, the measured dipole transfer function at 77 K is within 3.5% of the calculation. The measured b_3 is within 6 units and a_3 is within 1 unit of the calculation (both at 77 K). Magnetization-current effects caused the discrepancy in both the transfer function and allowed normal sextupole in the center region of the magnet at both 77 and 4.2 K.

The dipole transfer function at the magnet center measured at different ramp rates at 4.2 K is shown in figure 15. No pronounced ramp-rate dependence was observed. Magnetization-current effects caused not only large deviations from the geometric value (0.25 T kA^{-1}) at low currents but also the hysteresis between the up and down ramps [50]. A 4% (400 units) deviation was measured during the up-ramp branch at 1.4 kA (30% of SSP). The TF approached the geometric value starting from around 3.5 kA (75% of SSP) during the up ramp.

During the ramp-rate measurements as shown in figure 15, the current was held at 188 A (0.05 T aperture field) and 4 kA (1 T) for 60 s with a stability of 0.01% to

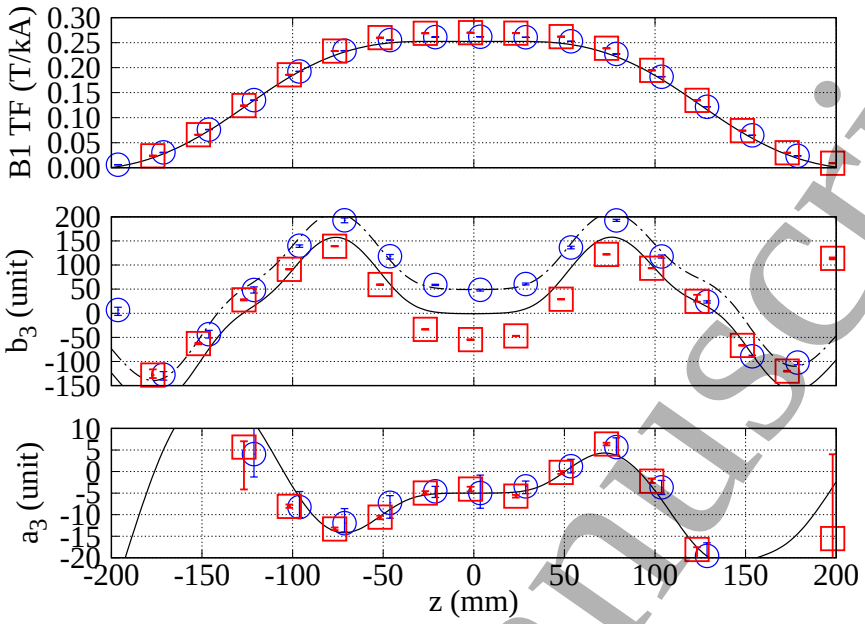

Figure 14. Comparison between the calculated (lines) and measured dipole transfer function and sextupoles at a current of 100 A at 77 K (blue circles) and 1 kA at 4.2 K (red squares). The b_3 calculation included a +50 unit shift of the calculation (dashed line). The calculated a_3 profile was shifted by −5 units. $R_{\text{ref}} = 21.55$ mm.

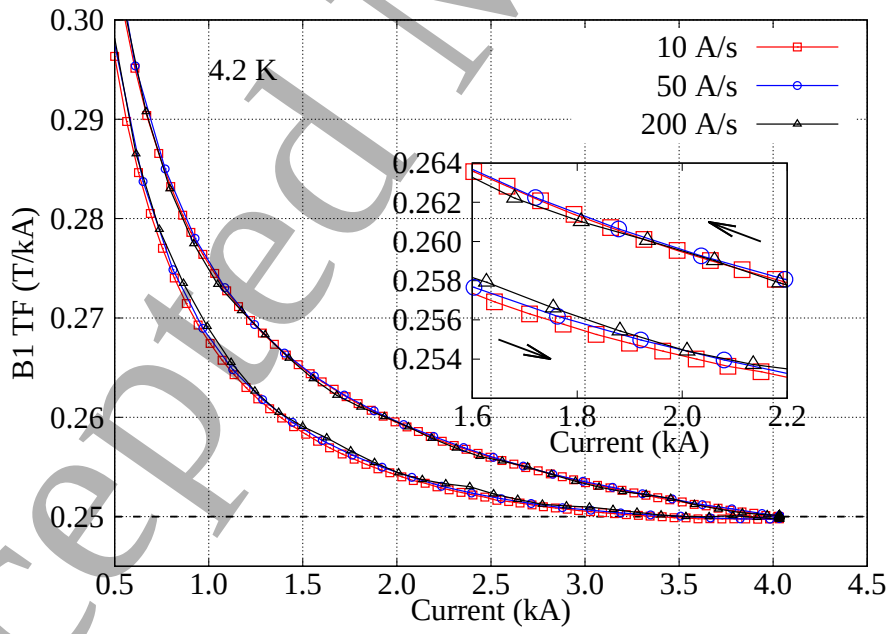

Figure 15. The dipole transfer function as a function of current and current ramp rates at 4.2 K. The dashed line indicates the expected transfer function of 0.25 T kA^{-1}. The ramp direction is indicated in the inset which also shows the negligible ramp-rate dependence.

measure the decay of the multipoles. Figure 16 shows the decay of the dipole transfer

function and b_3. The dipole transfer function was normalized to the geometric value 0.25 T kA^{-1}. Larger decays occurred at the 188 A plateau with a clear dependence on the current ramp rate. The observed decay can be described with a double-exponential fit (solid lines in figure 16) with a time constant ranging from 20 - 60 s.

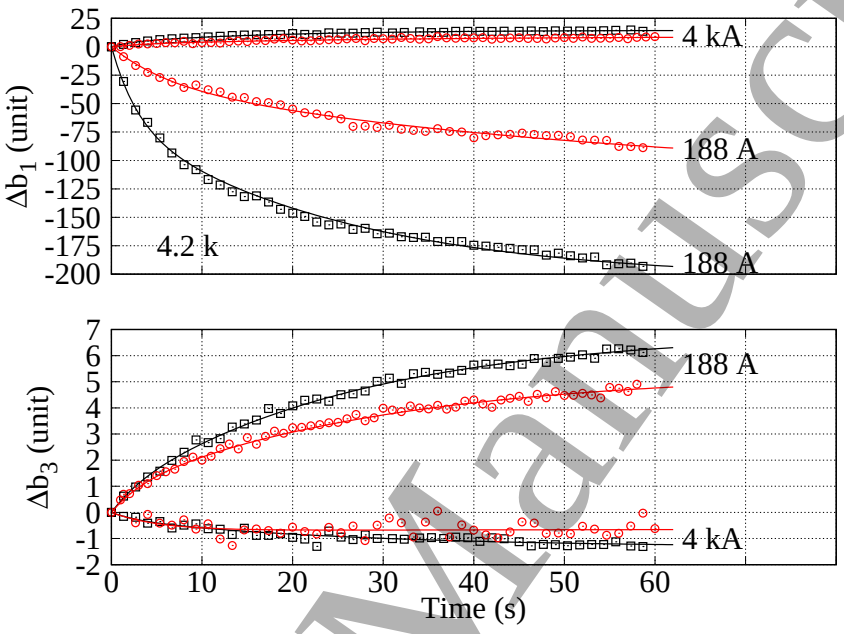

Figure 16. Change of the normalized dipole transfer function and normal sextupole measured during the first 60 s at 188 A and 4 kA, 4.2 K. Current ramped from 50 A to 4 kA and then down to 188 A. At time zero, current stopped ramping. Two ramp rates are shown: 20 As^{-1} (red circles) and 200 As^{-1} (black squares). Data were shifted in the y-axis to cancel the initial value.

5. Discussion

5.1. CCT concept with CORC® wires is scalable to larger accelerator magnets

The work reported here further demonstrated that CORC® CCT is a practical solution for HTS accelerator magnets. The reasonable magnet performance with the layer voltage onset at 81% of SSP suggested that the magnet fabrication technique was robust and caused no significant conductor degradation. The winding concept is also expected to be viable for longer magnets by horizontally positioning the mandrel that passes through the tilted winding wheel.

We note that 81% of SSP is conservative since the CORC® wire $I_c(B)$ performance was estimated based on the tape performance defined at 1 μV cm^{-1} which was about 1500 times higher than the criterion used to determine the magnet performance. We suggest future measurements of CORC® wire performance adopt a voltage criterion consistent with that is used for magnets.

The test result of individual layers after winding indicated that neither CORC® wire had any fatal defects. This was supported by the fact that the I_c of each layer at 77 K before and after assembly was consistent with earlier 3-turn magnets [32], considering higher self-fields in C1 due to larger number of conductor turns. The result was significant as C1 used two 15 m long CORC® wires, by far the longest pieces used in a magnet. It was a first important step toward demonstrating robust and uniform performance over long conductor length that is required for future high-field REBCO accelerator magnets.

The return-end joint of magnet C1 had a resistance (53 nΩ) consistent with previous 3-turn magnets (10 - 93 nΩ) [32]. The two individual terminations inside the return-end joint had different performance as evidenced by different transition currents. This could be caused by several factors such as slightly different locations of voltage taps within the terminations, different void volumes inside the terminations that was related to the soldering process and different surface conditions of Cu blocks, all can be improved for future magnets.

5.2. C1 demonstrated good transport performance with high thermal stability

C1 showed reasonably good transport performance with a peak current similar to the short-sample prediction without thermal runaway even with the resistive voltage across the layers and Joule heating originating from the terminations. High thermal stability was also observed in the impregnated aligned block magnet using Roebel cables tested in gas helium at 5 K [22]. Compared to NbTi and Nb_3Sn conductors with order-of-magnitude lower minimum quench energy [51], we expect that REBCO accelerator magnets will be immune to training that has been a lasting issue for low-temperature superconducting (LTS) accelerator magnets [2]. A similar remarkable thermal stability was also demonstrated in Bi2212 racetrack coils [3, 4].

C1 demonstrated robust transport performance against thermal cycles. Although we observed a slight decrease in the magnet transport performance (3%) at 77 K after four thermal cycles, this could have been caused by a re-positioning of the CORC® wires in the grooves or the change in the contact resistance inside terminations as shown in figure 13.

The magnet performance was limited by Layer 1, as expected from the higher magnetic fields on Layer 1. The voltage rise (V_2) in Layer 1 was likely caused by the in-field wire performance after winding as opposed to the heating inside the termination because Layer 2 had higher heating (50 μV peak voltage in V_1 *vs* 15 μV, figure 12) and yet it transitioned at a higher current than Layer 1 (4.094 kA *vs* 3.761 kA, figure 8).

5.3. C1 showed reasonable geometric field quality and further studies are required

Although the C1 magnet was developed to demonstrate the field generation, it provided a first opportunity to probe various aspects of the field quality for CCT dipole magnets using REBCO conductors.

C1 showed reasonable agreement with the as-designed conductor positioning at low field with minimal conductor movement. This suggested that CCT magnets using CORC® wires can deliver good geometric field quality, as expected for the CCT design [52]. Impregnating coils with epoxy for future coils is planned to reduce the impact of conductor movement under Lorentz forces.

The strong magnetization-current effects observed at low current can be a concern for both insert and stand-alone applications. Several potential solutions are available. On the conductor side, it was demonstrated that tape striations [53] reduces the magnetization-current effects in pancake coil configuration [54]. Aligning the flux lines with the tape broad surface to leverage the micron-thickness of REBCO layer has proved to be effective in CERN's Roebel dipole magnet [55]. On the magnet side, several passive correction methods based on superconductors and ferromagnetic shims can compensate the magnetization-current effects [56, 57]. Further study of the magnetizationx-current effects in CORC® wires and magnets in self-field and background fields is necessary as part of the wire optimization for use in accelerator magnets.

The decay of multipoles, measured over a limited duration of 60 s, suggested a current redistribution process inside the CORC® wire that depends on several factors such as the inter-tape contact, multi-layer wire architecture and local spatial and temporal field gradients. Understanding this process and the impact of inter-tape contact resistance on the competing needs between the dynamic field quality and current sharing between tapes will help establish an optimal range for the inter-tape contact resistance for accelerator magnet applications.

5.4. Open issues and next steps to demonstrate higher dipole fields

The C1 magnet highlighted the need of flexible CORC® wires. With an aperture of 70 mm, C1 had a large tilt angle of 40 degrees to keep the bending radius of the wire larger than 25 mm. As explained in [32], a large tilt angle compromises the magnet efficiency. It also leads to a large ratio of 1.2 between the peak field on the conductor and the field in the aperture.

Thinner tapes are key to improve the wire flexibility. CORC® wires that contain tapes with 30 micron substrates are between 3 mm and 4 mm thick depending on their operating current and J_e at 20 T, resulting in an allowable bending radius of between 20 and 30 mm. Thinner CORC® wires wound from tapes with 25 and 20 μm thick substrates are now being developed through a collaboration between SuperPower Inc. and ACT. Long CORC® wires containing tapes with 25 and 20 micron substrates are expected to become commercially available in 2019. These CORC® wires would allow operating currents of 5 - 10 kA at 20 T with J_e in the order of 500 – 700 A mm^{-2}. Their high in-field performance, together with their expected allowable bending radii of less than 20 mm would allow development of more efficient CORC® CCT magnets, which makes the ultimate goal of reaching a dipole field of 20 T within reach.

Strong mandrel and epoxy impregnation should be demonstrated to support

conductors against large Lorentz force for high-field magnet applications. Metal mandrels and their fabrication technology need to be developed to facilitate automated coil winding with minimum disturbance or handling on CORC® wires. Although the mechanical strength of CORC® wires already exceeds that of most LTS conductors and all other HTS cables, their strength can be further improved by for instance replacing the oxygen-free high-conductivity Cu former with a stronger copper alloy [25].

Better diagnostic capability is required to improve magnet fabrication technology. Although the voltage signals were effective to detect the superconducting to normal transitions for C1 and earlier magnets [32], they are insufficient to pinpoint the exact locations of normal zones inside the winding. This information is critical to understand and address the fabrication issues that limit magnet performances. The capability of measuring temperature and strain along magnet windings as demonstrated by fiber-optic based sensors [58] can be a promising solution. It can also benefit early detection of superconducting to the normal transition that will be critical for REBCO magnets featuring slow propagation of normal zones.

The peak current of C1 was suprisingly higher than the short-sample prediction by 5%. We suspect the uncertainty of the CORC® wire $I_c(B)$ estimated from the I_c of single tapes contributed to this issue [32]. Assessing the magnet fabrication technology requires a reliable prediction of the expected magnet performance. Assuming the performance of long magnet conductor can be represented by short CORC® wire samples, we need to measure the $I_c(B)$ of the short wire samples and use the same criterion to determine the wire I_c and magnet performance.

To address these development needs, we intend to continue developing and demonstrating CORC® CCT dipole magnets with higher dipole fields in collaboration with conductor vendors. The successful demonstrations will pave the way to develop high-field high-temperature superconducting accelerator magnets for inserts to enable 20 T dipole magnets for next-generation circular colliders and stand-alone magnets that can operate over a wide range of temperatures.

6. Conclusion

We successfully demonstrated the first high-temperature superconducting CCT dipole magnet using 30 m long commercial CORC® wires. The magnet design and fabrication was straightforward and no heat treatment was required. The magnet generated a peak dipole field of 1.2 T with 4.8 kA at 4.2 K, exceeding the initial goal of 1 T by 20%. The magnet showed high thermal stability at the peak current of 4.8 kA (618 A mm^{-2} at a minimum bending radius of 25 mm), similar to the short-sample prediction at 4.2 K. The magnet showed reasonable geometric field quality, despite not being impregnated to constrain conductor movement. The observed magnetization-current effects and multipole decay are a major issue that must be addressed in order to make accelerator magnets based on CCT and CORC® wires feasible. In this work, we demonstrated a promising path for high-temperature superconducting accelerator magnets for both

insert and stand-alone applications. It is a first step towards demonstrating the feasibilty to develop high-temperature superconducting accelerator magnets based on CCT design and CORC® wires to shift the paradigm for high-field accelerator magnet technology.

Acknowledgments

XRW thanks Tengming Shen for the SCXI digitizer to measure the voltage signals. We also thank Shlomo Caspi, Diego Arbelaez, Lucas Brouwer, Thomas Lipton for useful discussions; Jordan Taylor, Marcos Turqueti and Kai Zhang for the collaboration during magnet tests. We also thank the reviewers for their comments and suggestions that improve the paper.

This work was supported by the US Magnet Development Program through Director, Office of Science, Office of High Energy Physics, of the US Department of Energy under Contract No. DEAC02-05CH11231. The work at Advanced Conductor Technologies LLC was also supported by the US Department of Energy under contracts DE-SC0014009 and DE-SC0015775.

The authors have confirmed that any identifiable participants in this study have given their consent for publication.

References

[1] Van Sciver S W and Marken K R 2002 *Physics Today* 37

[2] Gourlay S A 2018 *Nucl. Instrum. Methods Phys. Res. A* **893** 124–137

[3] Zhang K, Higley H, Ye L, Gourlay S, Prestemon S, Shen T, Bosque E, English C, Jiang J, Kim Y, Lu J, Trociewitz U, Hellstrom E and Larbalestier D 2018 *Superconductor Science and Technology* **31** 105009

[4] Shen T, Jiang J, Bosque E, White M, Davis D, Zhang K, Higley H, Turqueti M, Huang Y, Miao H, Trociewitz U, Hellstrom E, Parrell J, Hunt A, Gourlay S, Prestemon S and Larbalestier D 2018 (*Preprint* `1808.02864`)

[5] Majkic G, Pratap R, Xu A, Galstyan E, Higley H, Prestemon S, Wang X, Abraimov D, Jaroszynski J and Selvamanickam V 2018 *Superconductor Science and Technology*

[6] Trociewitz U P, Dalban-Canassy M, Hannion M, Hilton D K, Jaroszynski J, Noyes P, Viouchkov Y, Weijers H W and Larbalestier D C 2011 *Applied Physics Letter* **99** 202506 (pages 3)

[7] Weijers H W, Markiewicz W D, Gavrilin A V, Voran A J, Viouchkov Y L, Gundlach S R, Noyes P D, Abraimov D V, Bai H, Hannahs S T and Murphy T P 2016 *IEEE Trans. Appl. Supercond.* **26** 4300807

[8] Yoon S, Kim J, Cheon K, Lee H, Hahn S and Moon S H 2016 *Superconductor Science and Technology* **29** 04LT04

[9] Hahn S 2017 Mini magnet packs world-record, one-two punch `https://nationalmaglab.org/news-events/news/mini-magnet-packs-world-record-punch`

[10] Bottura L and Godeke A 2012 *Reviews of Accelerator Science and Technology* **5** 25–50

[11] Goldacker W, Grilli F, Pardo E, Kario A, Schlachter S I and Vojenčiak M 2014 *Superconductor Science and Technology* **27** 093001

[12] Takayasu M, Chiesa L, Bromberg L and Minervini J V 2012 *Superconductor Science and Technology* **25** 014011

[13] Weiss J D, Mulder T, ten Kate H J and van der Laan D C 2017 *Superconductor Science and Technology* **30** 014002 and references therein.

[14] Zangenberg N, Nielsen G, Hauge N, Nielsen B, Baurichter A, Pedersen C, Brauner L, Ulsoe B and Moller S 2012 *IEEE Trans. Appl. Supercond.* **22** 4004004

[15] Amemiya N, Zhang Z, Sano T, Sogabe Y, Ogitsu T, Koyanagi K, Kurusu T, Mori Y, Iwata Y, Noda K and Yoshimoto M 2015 *IEEE Trans. Appl. Supercond.* **25** 4003505

[16] Gupta R, Anerella M, Ghosh A, Lalitha S, Sampson W, Schmalzle J, Kolonko J, Scanlan R, Weggel R, Willen E and Nakao K 2015 *IEEE Trans. Appl. Supercond.* **25** 4003704

[17] Koyanagi K, Takayama S, Miyazaki H, Tosaka T, Tasaki K, Kurusu T and Ishii Y 2015 *IEEE Trans. Appl. Supercond.* **25** 4003104

[18] Bogdanov I V, Kozub S S, Sytnik V V, Terskiy I S, Tkachenko L M, Trusov O V, Shirshov L S, Smirnov V M, Shuvalov V I, Shcherbakov P A, Molodyk A A, Lee S R and Samoilenkov S V 2016 *Superconductor Science and Technology* **29** 105012

[19] Rossi L, Badel A, Bajko M, Ballarino A, Bottura L, Dhalle M, Durante M, Fazilleau P, Fleiter J, Goldacker W, Härö E, Kario A, Kirby G, Lorin C, van Nugteren J, de Rijk G, Salmi T, Senatore C, Stenvall A, Tixador P, Usoskin A, Volpini G, Yang Y and Zangenberg N 2015 *IEEE Trans. Appl. Supercond.* **25** 4001007

[20] Badel A, Ballarino A, Barth C, Bottura L, Dhalle M M J, Fleiter J, Goldacker W, Himbele J, Kario A, Rossi L, Rutt A, Scheuerlein C, Senatore C, Tixador P, Usoskin A and Yang Y 2016 *IEEE Trans. Appl. Supercond.* **26** 4803908

[21] Kirby G, van Nugteren J, Ballarino A, Bottura L, Chouika N, Clement S, Datskov V, Fajardo L, Fleiter J, Gauthier R, Gentini L, Lambert L, Lopes M, Perez J, de Rijk G, Rijllart A, Rossi L, ten Kate H, Durante M, Fazilleau P, Lorin C, Haro E, Stenvall A, Caspi S, Marchevsky M, Goldacker W and Kario A 2015 *IEEE Trans. Appl. Supercond.* **25** 4000805

[22] van Nugteren J, Kirby G, Bajas H, Bajko M, Ballarino A, Bottura L, Chiuchiolo A, Contat P A, Dhallé M, Durante M, Fazilleau P, Fontalva A, Gao P, Goldacker W, ten Kate H, Kario A, Lahtinen V, Lorin C, Markelov A, Mazet J, Molodyk A, Murtomäki J, Long N, Perez J, Petrone C, Pincot F, de Rijk G, Rossi L,

Russenschuck S, Ruuskanen J, Schmitz K, Stenvall A, Usoskin A, Willering G and Yang Y 2018 *Superconductor Science and Technology* **31** 065002

[23] Durante M, Borgnolutti F, Bouziat D, Fazilleau P, Gheller J M, Molinié F and Antoni P D 2018 *IEEE Trans. Appl. Supercond.* **28** 4203805

[24] van der Laan D C, McRae D M and Weiss J D 2018 *Superconductor Science and Technology* **32** 015002

[25] DC van der Laan D M and Weiss J 2019 Effect of monotonic and cyclic axial tensile stress on the performance of superconducting CORC® wires

[26] Otten S, Dhallé M, Gao P, Wessel W, Kario A, Kling A and Goldacker W 2015 *Superconductor Science and Technology* **28** 065014

[27] van der Laan D C, Weiss J D and McRae D M 2019 *Superconductor Science and Technology* **32** 033001

[28] Kar S, Luo W, Ben Yahia A, Li X, Majkic G and Selvamanickam V 2018 *Superconductor Science and Technology* **31** 04LT01

[29] Gourlay S A, Prestemon S O, Zlobin A V, Cooley L and Larbalestier D 2016 The U.S. magnet development program plan `https://science.energy.gov/~/media/hep/pdf/Reports/MagnetDevelopmentProgramPlan.pdf`

[30] van der Laan D and Weiss J 2016 Progress in high-temperature superconducting corc accelerator magnet cable and wire development Presentation at the Low Temperature High Field Superconductor Workshop

[31] Weiss J, van der Laan D, Mulder T, Kate H T, Godeke A, Kolb-Bond D and Larbalestier D 2016 Enhanced flexibility of round high-temperature superconducting CORC wires for high-field magnet applications Presentation at the 8th Workshop on Mechanical and Electromagnetic Properties of Composite Superconductors (MEM16) `https://nationalmaglab.org/images/news_events/events/mem/talks/s2_weiss.pdf`

[32] Wang X, Caspi S, Dietderich D R, Ghiorso W B, Gourlay S A, Higley H C, Lin A, Prestemon S O, van der Laan D and Weiss J D 2018 *Superconductor Science and Technology* **31** 045007

[33] Piekarz H, Blowers J, Hays S and Shiltsev V 2014 *IEEE Trans. Appl. Supercond.* **24** 4001404

[34] Gupta R, Anerella M, Cozzolino J, Joshi P, Sampson W, Wanderer P and Zeller A 2015 *IEEE Trans. Appl. Supercond.* **25** 4603306

[35] Amemiya N, Goda K, Otake H, Nakamura T, Ogitsu T, Koyanagi K, Kurusu T, Mori Y, Iwata Y, Noda K *et al.* 2013 *IEEE Trans. Appl. Supercond.* **23** 4601905

[36] Meyer D and Flasck R 1970 *Nuclear Instruments and Methods* **80** 339–341

[37] Gavrilin A V, Bird M D, Bole S T and Eyssa Y M 2002 *IEEE Trans. Appl. Supercond.* **12** 465–469

[38] Goodzeit C L, Ball M J and Meinke R B 2003 *IEEE Trans. Appl. Supercond.* **13** 1365–1368

[39] Akhmeteli A M, Gavrilin A V and Marshall W S 2006 *Superconductivity, Magnetism and Magnets* (Nova Publishers) chap 5 and references therein.

[40] Caspi S, Borgnolutti F, Brouwer L, Cheng D, Dietderich D R, Felice H, Godeke A, Hafalia R, Martchevskii M, Prestemon S, Rochepault E, Swenson C and Wang X 2014 *IEEE Transactions on Applied Superconductivity* **24** 4001804 and references therein.

[41] Brouwer L N 2015 *Canted-Cosine-Theta Superconducting Accelerator Magnets for High Energy Physics and Ion Beam Cancer Therapy* Ph.D. thesis University of California, Berkeley

[42] Godeke A, Brouwer L N, Caspi S, Dietderich D R, Gourlay S A, Hafalia R R, Heys N I, Higley H C, Lipton T M, Reynolds M A and Swanson J H 2015 *IEEE Trans. Appl. Supercond.* **25** 4002404

[43] Garcia Fajardo L, Brouwer L, Caspi S, Gourlay S, Prestemon S and Shen T 2018 *IEEE Trans. Appl. Supercond.* **28** 4008305

[44] Caspi S, Brouwer L, Lipton T, Hafalia A, Prestemon S, Dietderich D, Felice H, Wang X, Rochepault E, Godeke A, Gourlay S and Marchevsky M 2015 *IEEE Trans. Appl. Supercond.* **25** 4000205

[45] Auchmann B, Brouwer L, Caspi S, Gao J, Montenero G, Negrazus M, Rolando G and Sanfilippo S 2018 *IEEE Trans. Appl. Supercond.* **28** 4000705

[46] Brouwer L, Caspi S, Hafalia R, Hodgkinson A, Prestemon S, Robin D and Wan W 2017 *IEEE Trans. Appl. Supercond.* **27** 4400106

[47] Kirby G A, Gentini L, Mazet J, Mentink M, Mangiarotti F, Van Nugteren J, Murtomäki J S, Hagen P, Pincot F O, Bourcey N, Perez J C, Rijk G D, Todesco E and Rysti J 2018 *IEEE Trans. Appl. Supercond.* **28** 4002205

[48] van der Laan D 2017 Superconducting cable connections and methods US Patent 9,755,329

[49] DiMarco J, Chlachidze G, Makulski A, Orris D, Tartaglia M, Tompkins J, Velev G and Wang X 2013 *IEEE Trans. Appl. Supercond.* **23** 9000505

[50] Mess K H, Schmüser P and Wolff S 1996 *Superconducting accelerator magnets* (World Scientific) chap 6

[51] Xu X, Li P, Zlobin A V and Peng X 2018 *Superconductor Science and Technology* **31** 03LT02

[52] Caspi S, Brouwer L N, Lipton T, Jr A H, Prestemon S, Dietderich D R, Felice H, Wang X, Rochepault E, Godeke A, Gourlay S and Marchevsky M 2015 *IEEE Trans. Appl. Supercond.* **25** 4002304

[53] Kesgin I, Levin G A, Haugan T J and Selvamanickam V 2013 *Appl. Phys. Lett.* **103** 252603

[54] Yanagisawa Y, Xu Y, Jin X, Nakagome H and Maeda H 2015 *IEEE Trans. Appl. Supercond.* **25** 6603705

[55] Petrone C, van Nugteren J, Bajas H, Bottura L, Kirby G, Rossi L and Russenschuck S 2018 *IEEE Trans. Appl. Supercond.* **28** 4604404

[56] Gilbert W, Borden A, Hassenzahl W, Moritz G and Taylor C 1985 *IEEE Trans. Magn.* **21** 486–489

[57] Kashikhin V and Zlobin A 2001 *IEEE Trans. Appl. Supercond.* **11** 2058–2061

[58] Scurti F, Ishmael S, Flanagan G and Schwartz J 2016 *Superconductor Science and Technology* **29** 03LT01